Iraqi Journal of Physics, 2021 *Vol.19, No.48, PP. 89-106*

DOI: 10.30723/ijp.19.48.89-106

Study of the Nuclear Structure of some Neutron Rich Si Isotopes Using Shell Model with Skyrme Interaction

Luma J. Abbas, Ali A. Alzubadi

Department of Physics, College of Science, University of Baghdad, Baghdad, Iraq

E-mail: ali.abdullatif@sc.uobaghdad.edu.iq

Corresponding author: Luam.jamal@duc.edu.iq

Abstract

The study of nuclear structure of neutron-rich nuclei acquired impressive interest internationally considering that it predicts nuclear behavior and reveals new aspects of nuclear structure that are the key challenges of developing a generalized nuclear model. In the present work, the nuclear structure of $^{28-40}$Si isotopes toward neutron dripline was investigated in the framework of shell model with Skyrme-Hrtree-Fock method using certain Skyrme parameterizations. Moreover, investigations of static properties such as nuclear densities for proton, neutron, mass, and, charge densities with their corresponding rms radii, neutron skin thicknesses, binding energies, separation energies, shell gap, and pairing gap were performed using the most recent Skyrme parameterization. For all dynamic properties, *sdpf* shell model space has been used to generate one body transition density matrix element with SDPFK two body effective interaction. The calculations also reproduced the low and higher-laying 2^+ energy level scheme, and reduced transition probability B(E2) for even Si-isotopes. The calculated results were compared with available experimental data, to identify which of these parameterizations introduced equivalent results with the experimental data and reasonable agreement was obtained.

Key words

Skyrme interaction, Skyrme-Hartree-Fock method, Si isotopes, neutron rich nuclei.

Article info.

Received: Oct. 2020
Accepted: Feb. 2021
Published: Mar. 2021

دراسة التركيب النووي لبعض نظائر Si الغنية بالنيوترونات باستخدام أنموذج القشرة مع تفاعل سكيرم

لمى جمال عباس، علي عبد اللطيف كريم

قسم الفيزياء، كلية العلوم، جامعة بغداد، بغداد، العراق

الخلاصة

حازت دراسة التركيب النووي للنويات الغنية بالنيوترونات على اهتمام دولي لقدرتها على التنبؤ بالسلوك النووي والكشف عن خصائص جديدة للتراكيب النووية والذي يشكل تحدي لتطويرأنموذج نووي عام. تمت دراسة التركيب النووي لنظائر نواة السيليكون $^{28-40}$Si باتجاه خط تقاطر النيوترونات في أطارانموذج القشرة النووي مع طريقة سكيرم هارتري- فوك باستخدام معلمات سكيرم. بالاضافة لذلك، تم دراسة الخصائص الساكنة مثل الكثافات النووية للبروتون والنيوترون والكتلة والشحنة مع انصاف الاقطار المقابلة لها، وايضا تمت دراسة كل من سمك القشرة النيوتروني، طاقات الربط، طاقات الفصل، فجوة القشرة وفجوة الاقتران باستخدام أحدث معلمات سكيرم. لجميع الخصائص الديناميكية، تم استخدم فضاء انموذج القشرة *sdpf* لتوليد عناصر مصفوفة انتقال الجسيم الواحد مع التفاعل الفعال بين الجسيمين من نوع SDPFK. كما تضمنت الحسابات دراسة مستويات الطاقة المنخفضة والعلوية للمستوي 2^+ واحتمالية الانتقال الكهربائي المختزلة B(E2) لنظائر Si الزوجية. أجريت مقارنة للنتائج المحسوبة مع القيم العملية المتوفرة لمعرفة المعلمات التي تعطي نتائج مقاربة ومكافئة للقيم العملية ووجد أن هنالك تقارب جيد بينهما.

Introduction

The study of nuclear structure of neutron-rich nuclei acquired impressive interest internationally for both experimental and theoretical sides. This is because it predicts nuclear behavior and reveals new aspects of nuclear structure that are the key challenges of developing a generalized nuclear model. These nuclei can be described as excitation modes that have distinctive structure over the structure or shape of the nuclear ground state. Moreover, the infrastructure of our earlier understanding of nuclei comes from shell structure and excitation modes. Extrapolation of the region near the dripline provides knowledge about modified features of nuclei such as magic number, shell gap and pairing gap. The theoretical estimation of the ground-state properties of nuclei near the neutron dripline is typically made in the framework of mean-field approaches; for instance, Hartree-Fock (HF) approximation. The Skyrme - Hartree- Fock (SHF) model is considered a powerful tool to describe the nuclear ground state. Furthermore, the inclusion of the parameterizations of Skyrme interaction provides an excellent description for nuclei up toward the vicinity of stability [1, 2].

The various nuclear density distributions with their corresponding root-mean-square (rms) radii and the neutron-skin provide essential information on nuclear structure. Furthermore, to extrapolate the properties of nuclei we should describe their shell structure with full information regarding binding energy and nuclear pairing, in addition to their separation energy, pairing energies and shell gap [3, 4].

Several studies have been performed to investigate the static and dynamic properties of Si isotopes. The excitation energies, B(E2), and S_{2n} for neutron-rich Si from N=22 to N=28 isotopic chain was investigated by Utsuno et al. [5]. The level scheme and B(E2) of ^{36}Si have been studied by Liang et al. [6] using SDPF-NR interaction. The comparison between excitation energies and B(E2) was identified by Ibbotson et al. for ^{32,34,36,38} Si-isotopes [7]. Energies of low lying, B(E2), S_{2n}, and S_{2p} have been studied by Cottle and Kemper in order to identify the subshell closure in N=20 and N=28 by examining S_{2n} [8]. Excited states for Si neutron-rich nuclei have been studied using *sd* shell model as well as the binding energies by Cole et al. [9]. Caurier et al. identified the low-lying states and B(E2) for ^{34}Si has been identified using SDPF-U interaction and comparison with experimental data showed excellent agreement [10].

The present work is divided into three sections, the first section displays charge, neutron, proton density, and root mean square radii of $^{28\text{-}40}$Si isotopes toward neutron dripline in framework of shell model with Skx25 Skyrme parameterizations. The second section is deployed to calculate the binding energies and nuclear pairing of $^{28\text{-}40}$Si isotopes. Third part is deploy to exhibit energy levels and reduced transition probability for low and higher-lying 2^+ states in even-even $^{28\text{-}40}$Si isotopes up toward neutron dripline. The calculations were performed with *sdpf* shell model space and SDPFK two-body effective interaction and it will be compared with the available experimental data.

Theoretical framework

The Skyrme effective interaction was developed from the postulation that the energy functional could be expressed in terms of a zero-range expansion, leading to a simple derivation of the HF equations. The two-body terms are written as a short-range expansion in the form [11-14].

$$V_{Skyrme}(\vec{r}_1,\vec{r}_2) = t_0(1+x_0\hat{P}_\sigma)\delta_{12} + \frac{t_1}{2}(1+x_1\hat{P}_\sigma)\left[\vec{k}'^2\delta_{12} + \delta_{12}\vec{k}^2\right]$$
$$+ t_2(1+x_2\hat{P}_\sigma)\vec{k}'\delta_{12}\vec{k} + \frac{t_3}{6}(1+x_3\hat{P}_\sigma)\rho\left(\frac{\vec{r}_1+\vec{r}_2}{2}\right)^\alpha \delta_{12} + iW_0\ \vec{k}'\delta_{12}(\vec{\hat{\sigma}}_1+\vec{\hat{\sigma}}_2)\times\vec{k}$$
$$+ \frac{t_e}{2}\left(\left[3\,(\vec{\hat{\sigma}}_1.\vec{k}')\,(\vec{\hat{\sigma}}_2.\vec{k}') - (\vec{\hat{\sigma}}_1.\vec{\hat{\sigma}}_2)\vec{k}'^2\right]\delta_{12} + \delta_{12}\left[3(\vec{\hat{\sigma}}_1.\vec{k})\,(\vec{\hat{\sigma}}_2.\vec{k}) - (\vec{\hat{\sigma}}_1.\vec{\hat{\sigma}}_2)\vec{k}^2\right]\right)$$
$$+ t_0\left[3(\vec{\hat{\sigma}}_1.\vec{k})\delta_{12}(\vec{\hat{\sigma}}_2.\vec{k}) - (\vec{\hat{\sigma}}_1.\vec{\hat{\sigma}}_2)\vec{k}'\delta_{12}\vec{k}\right] \quad \textbf{(1)}$$

where $\delta_{12} = \delta(\vec{r}_1 - \vec{r}_2)$ and *k*, *k*′ are the relative momentum operators with *k* acting on the right, while *k*′ is the operator acting on the left and are given by:

$$\hat{k}' = -\frac{1}{2i}(\vec{\nabla}_1 - \vec{\nabla}_2),\ \hat{k} = \frac{1}{2i}(\vec{\nabla}_1 - \vec{\nabla}_2), \quad \textbf{(2)}$$

also, $\hat{P}_\sigma$ is the spin-exchange operator that are given as:

$$\hat{P}_\sigma = \frac{1}{2}(1+\hat{\sigma}_1\cdot\hat{\sigma}_2) \quad \textbf{(3)}$$

where $\hat{\sigma}$ are the Pauli spin matrices. The Skyrme parameterizations; x_n, t_n, t_o, t_e, α and W_0 are the free parameters, that are must be fitted to nuclear structure experimental data. Each term creates both time-even and time-odd densities in the HF equations [15].

The overall many-body Hamiltonian is written in term of kinetic energy and nucleon-nucleon interaction.

$$\boldsymbol{\hat{H} = -\sum_{i=1}^{A}\frac{\hbar^2}{2m}\nabla^2 + \frac{1}{2}\sum_{i\neq j}^{A} v(i,j)} \quad \textbf{(4)}$$

According to SHF approximation, the total binding energy of the system is given by the sum of Coulomb energy, kinetic energy and Skyrme energy, which describe the effective interaction between nucleons

$$\boldsymbol{E = E_{Coul} + E_{kin} + \int E_{Sky}d^3r + E_{pair}} \quad \textbf{(5)}$$

By substituting the Skyrme interaction terms into the full energy expression, the total energy of the system can be written as [14]:

$$\boldsymbol{\langle\Phi_{HF}|\hat{H}|\Phi_{HF}\rangle = -\frac{\hbar^2}{2m}\sum_{i=1}^{A}\int \phi_i^*(r_1)\nabla_i^2\phi_i(r_1)dr_1}$$
$$\boldsymbol{+\frac{1}{2}\sum_{ij\sigma_1\sigma_2q_1q_2}^{A}\iint d^3r_1d^3r_2\phi_i^*(r_1,\sigma_1,q_1)\phi_j^*(r_2,\sigma_2,q_2)\,v(r_1,r_2)}$$

$$\boldsymbol{\left(1-\hat{P}_M\hat{P}_\sigma\hat{P}_q\right)\phi_i(r_1,\sigma_1,q_1)\phi_j(r_2,\sigma_2,q_2)} \quad \textbf{(6)}$$

The densities ρ(r) in spherical representation are given by:

$$\boldsymbol{\rho_q(r) = \sum_{n_\beta j_\beta l_\beta} \omega_\beta \frac{2j_\beta+1}{4\pi}\left(\frac{R_\beta}{r}\right)^2}, \quad \textbf{(7)}$$

where $\left(\frac{R_\beta}{r}\right)$ represent redial part, q represents one of the following; neutron, proton and charge, ω_β is the occupation probability of the state β and j_β is the total angular momentum of single particle ($j_\beta = l_\beta + s$), that vanishes for ground states.

The rms radii of neutron, proton, charge, and mass distributions can be evaluated from these densities as [16, 17]:

$$\boldsymbol{r_q = \langle r_q^2 \rangle^{1/2} = \left[\frac{\int r^2 \rho_q(r) dr}{\int \rho_q(r) dr}\right]^{1/2}} \quad \textbf{(8)}$$

A quantity providing information about the structure of the nuclei is the neutron skin thickness t, which can then be defined as the difference between the neutron rms radius and the proton rms radius [17]:

$$\boldsymbol{\Delta r_{np} = \langle r^2 \rangle_n^{1/2} - \langle r^2 \rangle_p^{1/2}} \quad \textbf{(9)}$$

The separation energies are mainly expressed in terms of the difference in binding energies then S denotes [18].

$$\boldsymbol{S_n = -Q_n = B(N,Z) - B(N-1,Z)} \quad \textbf{(10)}$$

$$\boldsymbol{S_{2n} = -Q_{2n} = B(N,Z) - B(N-2,Z)} \quad \textbf{(11)}$$

The shell gaps in nuclei are defined as the sum of the neutron and proton shell gaps based on the difference of the binding energies [15].

$$\boldsymbol{\Delta(N,Z) = \Delta n(N,Z) + \Delta p(N,Z)} \quad \textbf{(12)}$$

$$\boldsymbol{\Delta n(N,Z) = B(N+2,Z) + B(N-2,Z) - 2B(N,Z)} \quad \textbf{(13)}$$

$$\boldsymbol{\Delta p(N,Z) = B(N,Z+2) + B(N,Z-2) - 2B(N,Z)} \quad \textbf{(14)}$$

where Δn is the neutron shell is gap and Δp is the proton shell gap.

While the two neutron separation energies may reveal some information about the structural changes, one may also get interesting information by calculating other type of binding energy differences, thus, the value of the two-neutron shell gap δ_{2n} is determined by:

$$\boldsymbol{\delta_{2n} = S_{2n}(Z,N) - S_{2n}(Z,N+2)} \quad \textbf{(15)}$$

The odd and even neutron pairing gap is defined as [15, 18, 19]

$$\boldsymbol{\Delta N^{(3)} = \frac{1}{2}(B(Z,N+1) - 2B(Z,N) + B(Z,N-1))} \quad \textbf{for N odd (16.1)}$$

$$\boldsymbol{\Delta N^{(3)} = -\frac{1}{2}(B(Z,N+1) - 2B(Z,N) + B(Z,N-1))} \quad \textbf{for N even (16.2)}$$

The many particles reduced matrix element of the electric multipole transition operator for an A-particle model space wave function of multipolarity λ is expressed as the sum of the product over the one-body density matrix (OBDM) elements times reduced Single-particle matrix elements, and is given by

$$\left\langle f \left\| \hat{T}^{\lambda} \right\| i \right\rangle = \left\langle n\omega_f J_f \left\| \hat{T}^{\lambda} \right\| n\omega_i J_i \right\rangle$$

$$= \sum_{k\alpha k\beta} OBDM(f,i,k_\alpha,k_\beta,\lambda) \left\langle k_\alpha \left\| \hat{T}^{\lambda} \right\| k_\beta \right\rangle \quad \textbf{(17)}$$

where k_i, k_f are single –particle state for initial and final model space state (nw_iJ_i) and (nw_fJ_f) respectively. Also ω indicates indices to differentiate between various states having the same J values. Giving rise to formalism of OBDM in the proton-neutron as follows [10].

$$OBDM(f,i,k_{\alpha,t_z},k_{\beta,t_z},\lambda)=\frac{\left\langle n\omega_f J_f \left\| \left[a^{+}_{k\alpha,tz} \otimes \tilde{a}_{k\beta,tz} \right]^{\lambda} \right\| n\omega_i J_i \right\rangle}{\sqrt{2\lambda+1}} \quad (18)$$

where t_z=1/2 for neutron and t_z=-1/2 for proton.
The reduced electric transition probability $B(EJ)$ in terms of the reduced many-particle matrix element of the electric transition operator is defined as [19]

$$B(EJ)=\frac{\left[(2J+1)!!\right]^2}{k^{2J}}\frac{\left|\left\langle J_f \left|\left| \hat{T}^{el}_J \right|\right| J_i \right\rangle\right|^2}{2J_i+1} \quad (19)$$

where k is the wave number. The reduced electric transition probability is in units of $e^2.fm^{2J}$.

Results and discussion

In the present research, all the theoretical calculations was performed using the NushellX@MSU shell model code [20]. The discussion of the results is divided into two parts, static and dynamic properties. The static nuclear properties to be investigated include; charge, proton, and neutron densities with their associated rms radii, binding and separation energies, pairing gap, and neutron skin thickness for the selected chain of Si-isotopes. Whereas, the dynamic properties is devoted to outlining the excitation energies and reduced transition probability B(E2).

1. Nuclear density and root mean square radii

The calculated charge density distributions for Si-isotopes are illustrated in Fig.1, from ^{28}Si to ^{34} Si, the calculations predict that adding additional neutrons results in a difference in charge density mainly in the interior of the nucleus. Moving to the more neutron-rich isotopes ^{34}Si to ^{40}Si the discrepancies (The deviation increase up to 0.6% with experimental values) are in the region near the center and a clear indication of a neutron skin is observed in the ground state densities. In Fig.2 the contour plots of neutron densities of Si-isotopes are depicted. The central part of the neutron density reaches its maximum value in the interior region and becomes smaller in the peripherals regions. Fig.3 illustrates the proton density distributions of Si-isotopes in which lighter color represents the lower values for density and darker color represents the higher density values. It is clear that the proton density for ^{34}Si, which has N=20 magic number exhibits a central depletion, but less pronounced than that of ^{40}Si which has N=28 magic number reflecting the partial filling of $2S_{1/2}$ level. Maximum depletion for the whole chain of Si-isotopes that appears for N=20 (^{34}Si) and N=26(^{40}Si) as obvious in Fig.3 was at the central part and is less dense than at the outer region, which implies the formation of bubble-like structure, Whereas the charge density does not show any depletion in the central region as shown in Fig.2.

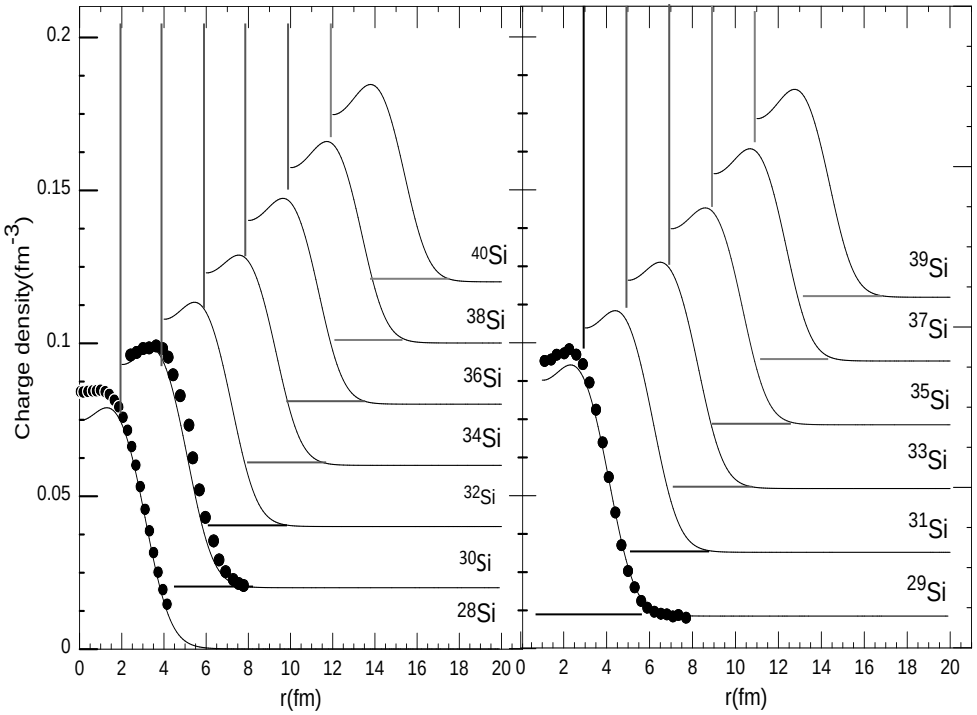

Fig.1: The calculated charge density distribution for Si-isotopes using Skxs25 parameterization in comparison with experimental data taken from Ref [21-23]. The charge-density units are in fm^{-3}. Beyond ^{28}Si the curves and data have been progressively offset by 1 fm and 0.01 in the charge density.

Fig.4 shows the point neutron, proton, charge, and total densities for the Si-isotopes under consideration using Skx25 parameterization in which the experimental charge density distribution data is available. In all plots, the mass point density is the same on both sides of the y-axis. The left-hand sides give the neutron density and the right-hand sides show the proton density as well as the charge density and, the experimental data. It is obvious that there is a visible discrepancy in the charge densities, particularly in the central region, which occur due to the error in the Fourier transform of theoretical data compared with experimental data. The scale on all the plots is the same and it is easily seen that the central total densities for all these isotopes lie around the expected region.

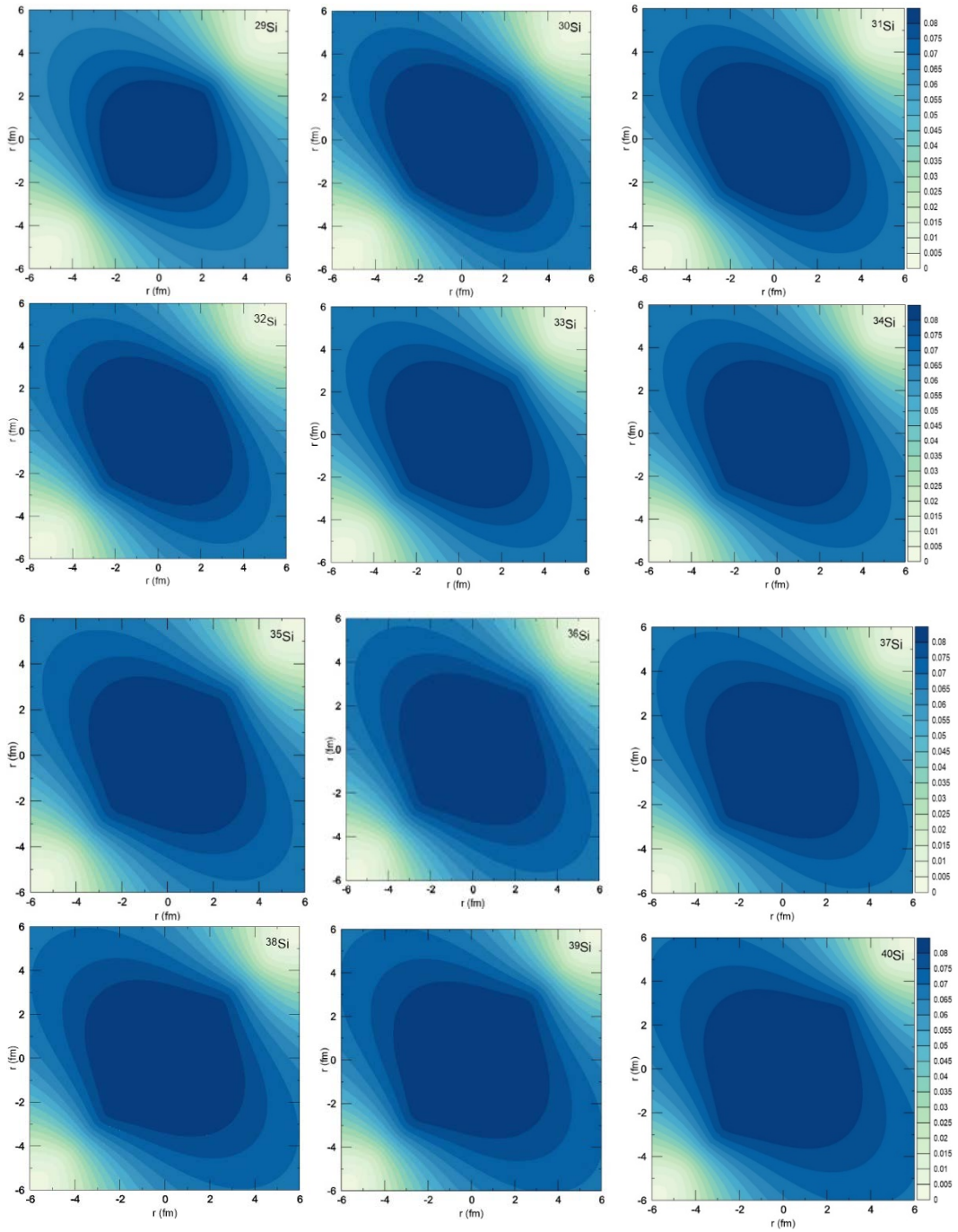

Fig.2: Contour plots of neutron density for Si-isotopes. The dark blue refers to high density regions, whereas, light green refers to minimum density regions as shows in the scale. The contour lines are drawn in a square box of dimension = 6 fm.

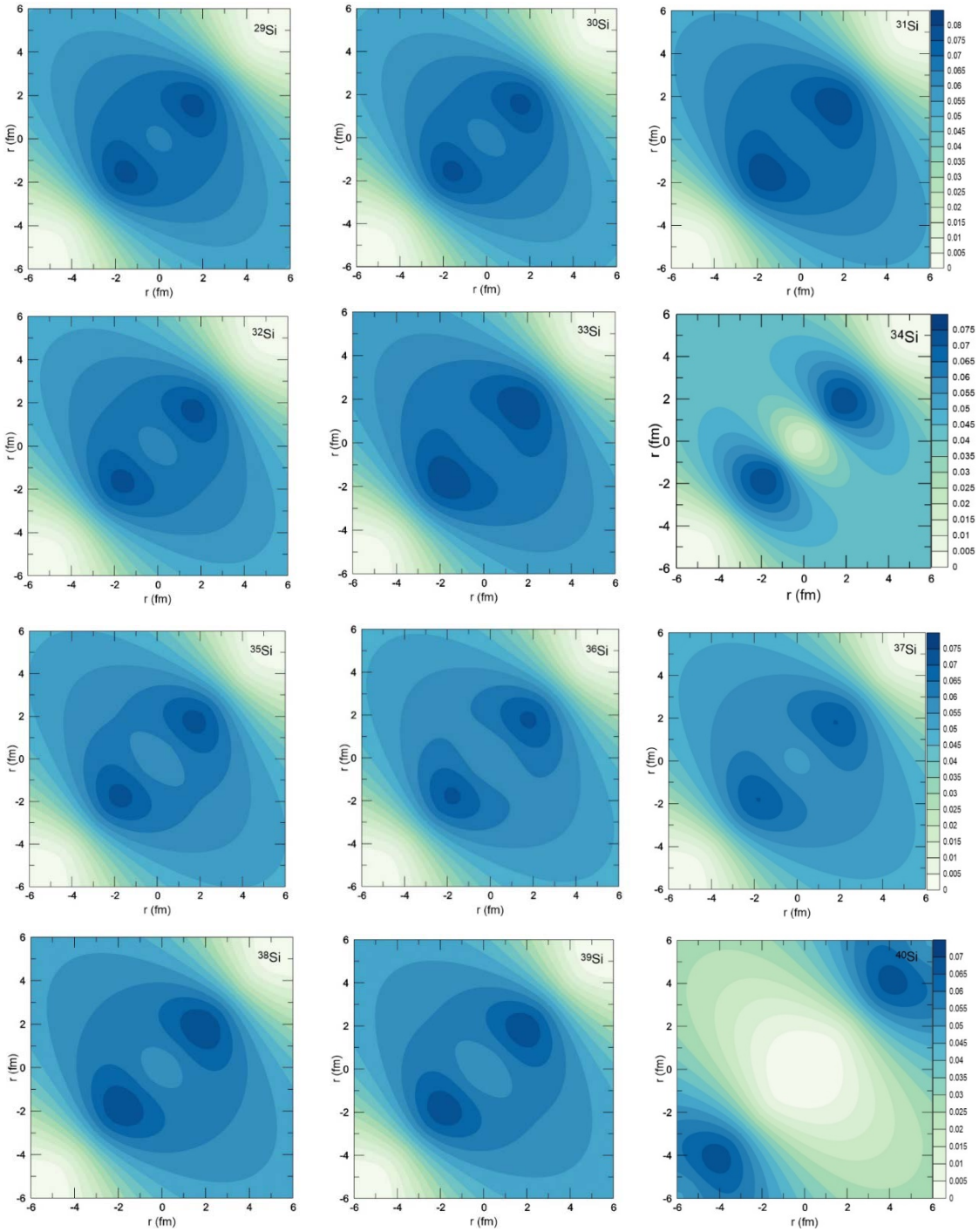

Fig.3: Contour plots of proton density for Si isotopes. The dark blue refers to high density regions, whereas, light green refers to minimum density regions as shows in the scale. The contour lines are drawn in a square box of dimension = 6 fm.

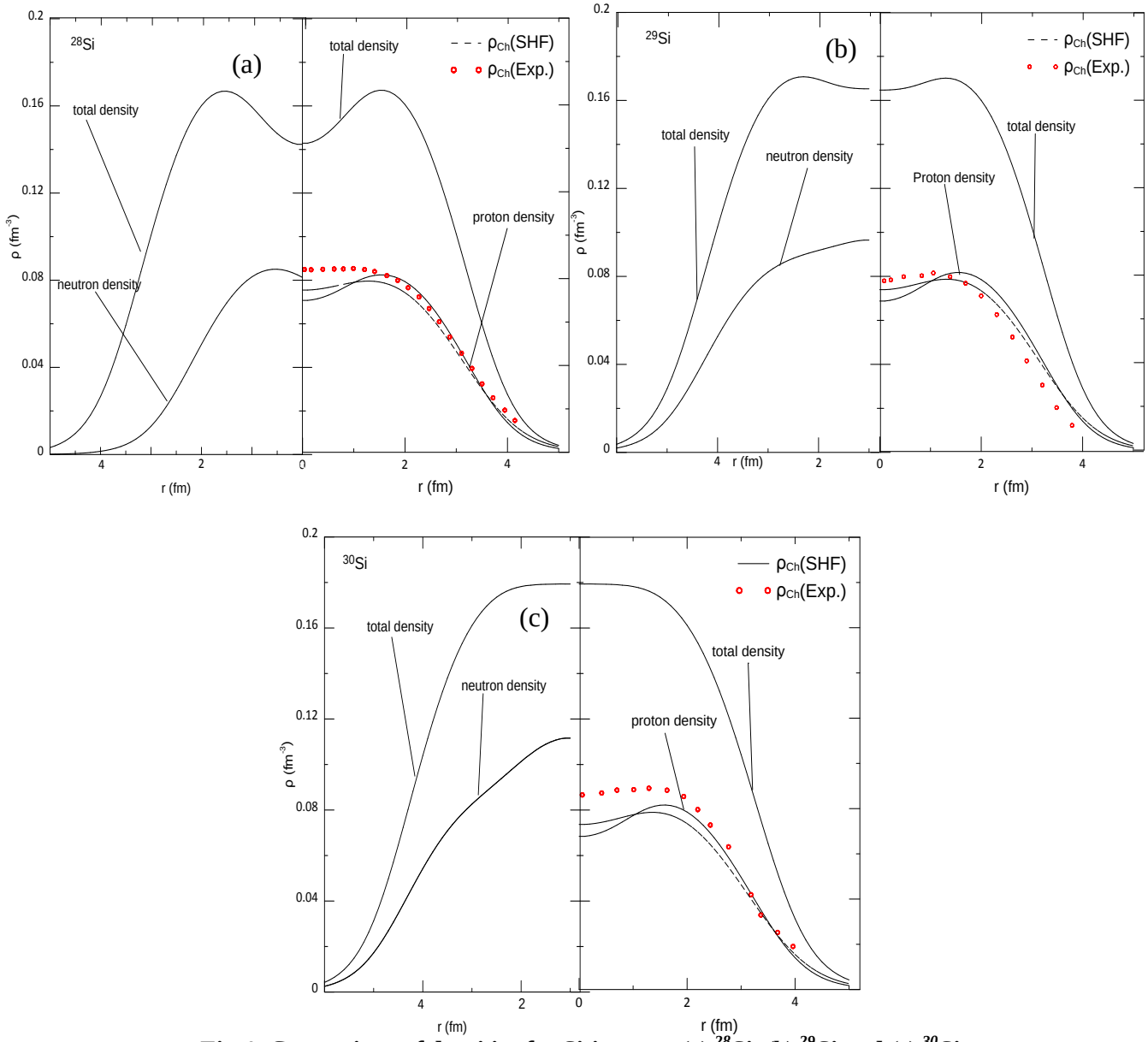

Fig.4: Comparison of densities for Si-isotopes (a) ^{28}Si, (b) ^{29}Si and (c) ^{30}Si.

The calculated rms charge radii for Si-isotopes are tabulated in Table 1 together with the available experimental data for those isotopes wherever it exists. The results also presented graphically in Fig.5. It is obvious that, the nuclei located near the vicinity of the dripline tend to have larger charge radius comparable to the stable one. The lowest value of charge radius is for ^{28}Si nucleus with N equals Z = 14 which signifies to shell closure with $1d_{5/2}$ occupation. Minimum values of the charge radii refer to the stable isotope and it is the point where the asymmetry and the Coulomb term originate the supreme balanced position that delivers the optimum nucleus stability. Fig.6 shows the proton, neutron and mass rms radii for Si isotopes. The calculated values show an unsteady increase of rms radii with the number of neutrons. Simultaneously, the values increase less rapidly at N=20(^{34}Si). Consequently, systematic differences occur between the neutron and proton rms radii.

Table 1: The calculated rms charge radii in (fm) for Si-isotopes in comparison with the experimental data taken from Ref. [24].

Isotope	SKx25	SLy4	Exp. [24]
^{28}Si	3.158	3.136	3.122
^{29}Si	3.156	3.143	3.1176
^{30}Si	3.157	3.151	3.133
^{31}Si	3.176	3.17	
^{32}Si	3.195	3.189	
^{33}Si	3.215	3.207	
^{34}Si	3.235	3.226	
^{35}Si	3.236	3.231	
^{36}Si	3.239	3.236	
^{37}Si	3.243	3.242	
^{38}Si	3.247	3.246	
^{39}Si	3.251	3.251	
^{40}Si	3.256	3.256	

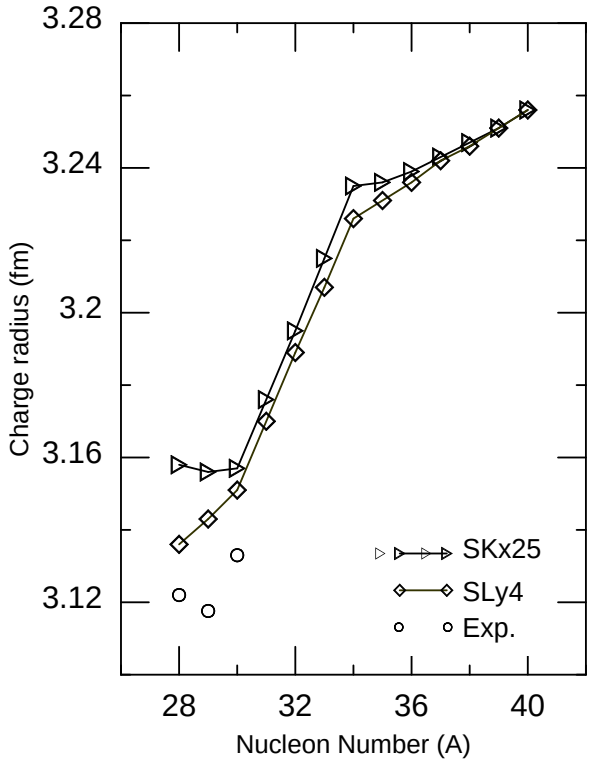

Fig.5: The nuclear rms charge radii for Si- isotopes as a function of nucleon number A in comparison with experimental data taken from Ref. [24].

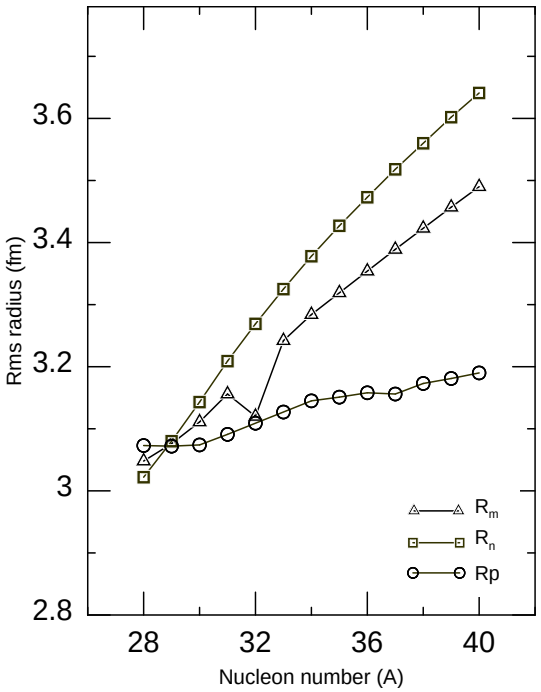

Fig.6 The neutron, proton, and mass rms radii for Si-isotopes as a function of nucleon number A calculated using Skx25 parameterization.

2. Nuclear binding energy and nuclear pairing

The total nuclear binding energies of the Si-isotopes are plotted against the nucleon number A as shown in Fig.7 using Skx25 parameterization. It is obvious that the calculated energies follow the general trend of the experimental data. Furthermore, it is clear that there is a sharp increase in binding energy observed between A=28 to A=33, because neutrons start to fill the $2s_{1/2}$ orbit and $1d_{3/2}$ which both are less bound than $1d_{5/2}$. However, starting to observe less increase in binding energy at this point up to the dripline where the binding energy curve becomes almost flat. There is excellent agreement between theoretical and experimental data is noticed with 1.2 MeV average discrepancies for both stable nuclei and those near the valley of stability. This leads to the conclusion that the SKx25 interaction is 1 to 1.2 MeV more bound than the experimental data. This occurs due to the residual interaction which becomes weaker toward the neutron dripline. This expresses the continuously decreasing binding energy needed to remove a pair of nucleons out of a given nucleus.

The one neutron separation energy for $^{28\text{-}39}$Si-isotopes are shown in Fig.8. Obviously, there is good energy agreement between calculated and experimental calculations. The largest discrepancy is found in A=38, and A=39 where the theoretical data is larger than experimental ones, which refer to strong pairing interaction. But in fact, the pairing properties of nuclei near the neutron dripline (where separation energy goes to zero) are similar to those near the valley of stability. It can be seen from the one neutron separation energy variation that ^{30}Si (N=16) and ^{36}Si (N=22) have higher value in comparison with adjacent isotopes which give indication of a new magic number and shell closure.

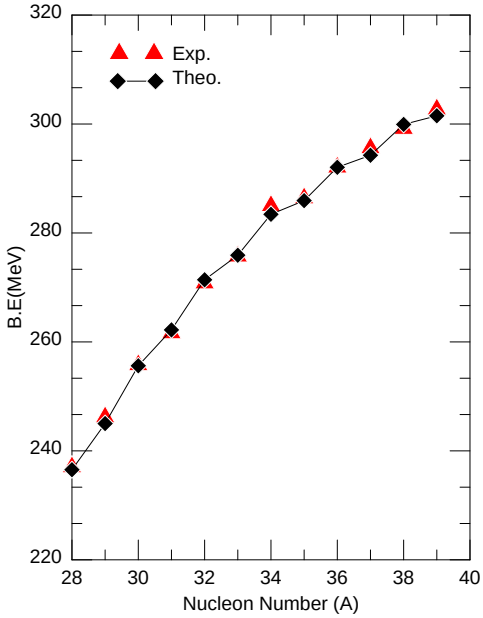

Fig.7: The calculated binding energies of Si-isotopes using SHF as a function of nucleon number A in comparison with experimental data taken from Ref. [25].

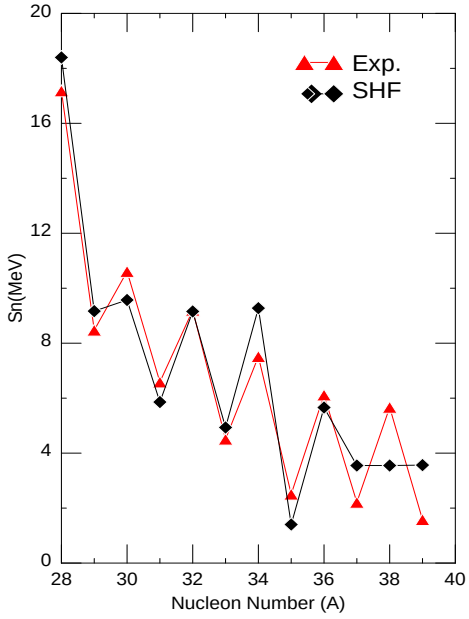

Fig.8: The calculated one neutron separation energy of Si-isotopes as a function of nucleon number A A in comparison with experimental data taken from Ref. [25].

The calculated two neutron separation energies are shown in Fig.9. The agreement between the experiment and theoretical calculation is quite good within ~ 1MeV, except for the N=20 with a discrepancy of ~ 2MeV due to the mixing of intruder configuration in ^{34}Si. Consequently, a high decrease of two neutron separation energy indicates that the parent nucleus is stable and less energy is needed to remove neutrons from the residue nuclei. Also, the results revealed that the two-neutron separation energy for ^{30}Si(N=16) and ^{36}Si (N=22) have relatively higher values than adjacent isotopes which indicates of magicity and shell closure. The particle stability of nuclei is directly related to the nuclear binding energies, which are very sensitive to the existence of shells and may provide clear signatures of shell closure. The shell gap

of the last two neutrons is displayed in Fig.10. The sharp drop of the two neutron shell gap δ_{2n} for N=20, N=22 is evidence of shell closure [26-29].

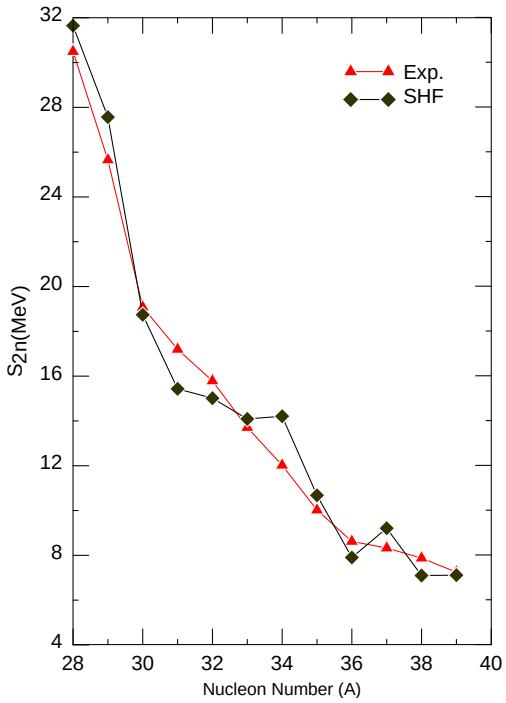

Fig.9: The calculated two neutron separation energy of Si-isotopes using SHF in comparison with experimental data taken from Ref. [25].

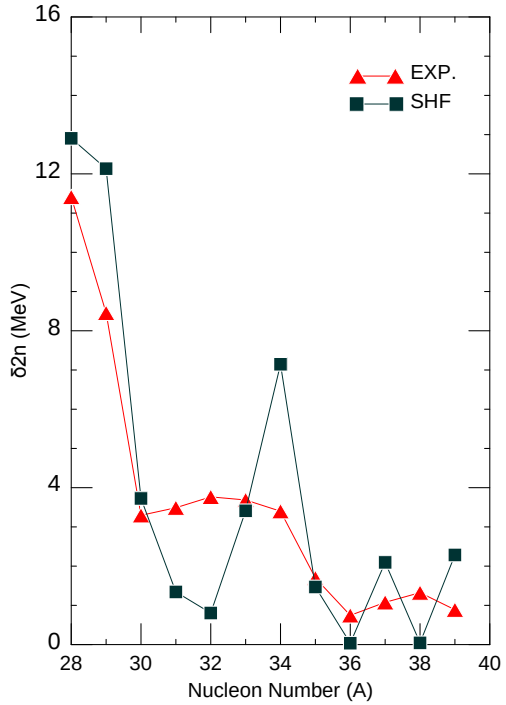

Fig.10: The calculated two neutron shell gap δ_{2n} of Si-isotopes as a function of nucleon number A in comparison with experimental data taken from Ref. [25].

Fig.11 shows pairing gap $\Delta 3n$ as a function nucleon number (A), it turns out that the lowest value for $\Delta 3n$ is observed in all nuclei with an even neutron number N. It is clear that the calculated shell gaps are in good agreement with experimental data. Moreover, ^{30}Si and ^{36}Si have higher values of pairing gap compared with neighboring isotopes due to the magicity and shell closure for N=16 and N=22. Fig.12 illustrates the neutron skin thickness Rn-Rp, plotted as a function of the nucleon number for Si isotopes. In this isotopic chain, we get the maximum value of a Rn-Rp as 0.352–0.417 fm for ^{37}Si to ^{40}Si which occur due to 1f7/2 occupation. More specifically, the neutron skin arises because the distribution of neutrons extends out further in radius than the proton distribution.

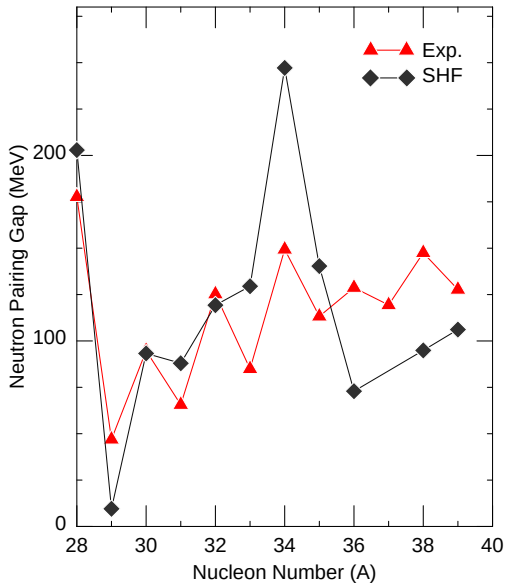

Fig.11: The calculated neutron pairing gap as a function of nucleon number A in comparison with experimental data taken from Ref. [25].

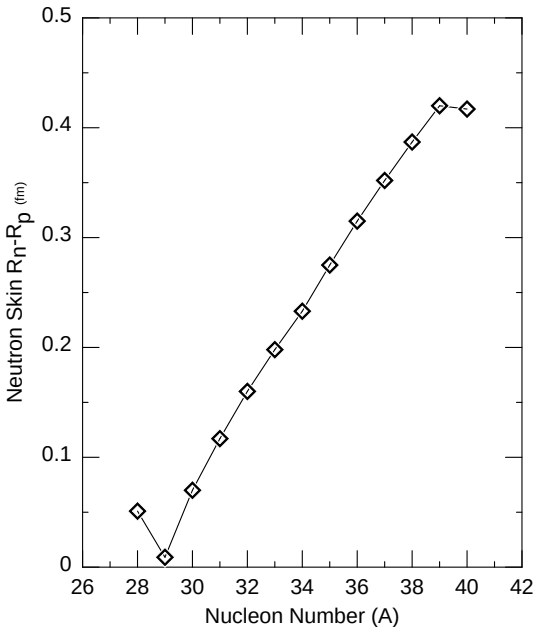

Fig.12: The neutron skin thickness Rn-Rp, versus the nucleon number of Si isotopes.

3. Energy levels and reduced transition probability

Fig.13 shows the calculated energy level scheme for low and higher-lying 2^+ states in even-even Si-isotopes. The calculations were performed with *sdpf* shell model space and SDPFK two-body effective interaction and were compared with the experimental data. One finds that the agreements between calculated energy levels and the experimental data are fairly good. The first excited 2^+ energy increases slightly with increasing neutron number for ^{28}Si to ^{34}Si until ^{34}Si is reached where the value start to increase sharply up to 4.968 MeV and then the value starts to decrease again in ^{36}Si to ^{38}Si which indicates that N=22 is shell closure [30-34] and the gap grows with increasing neutron number due to n-n interaction resulting in shell gap.

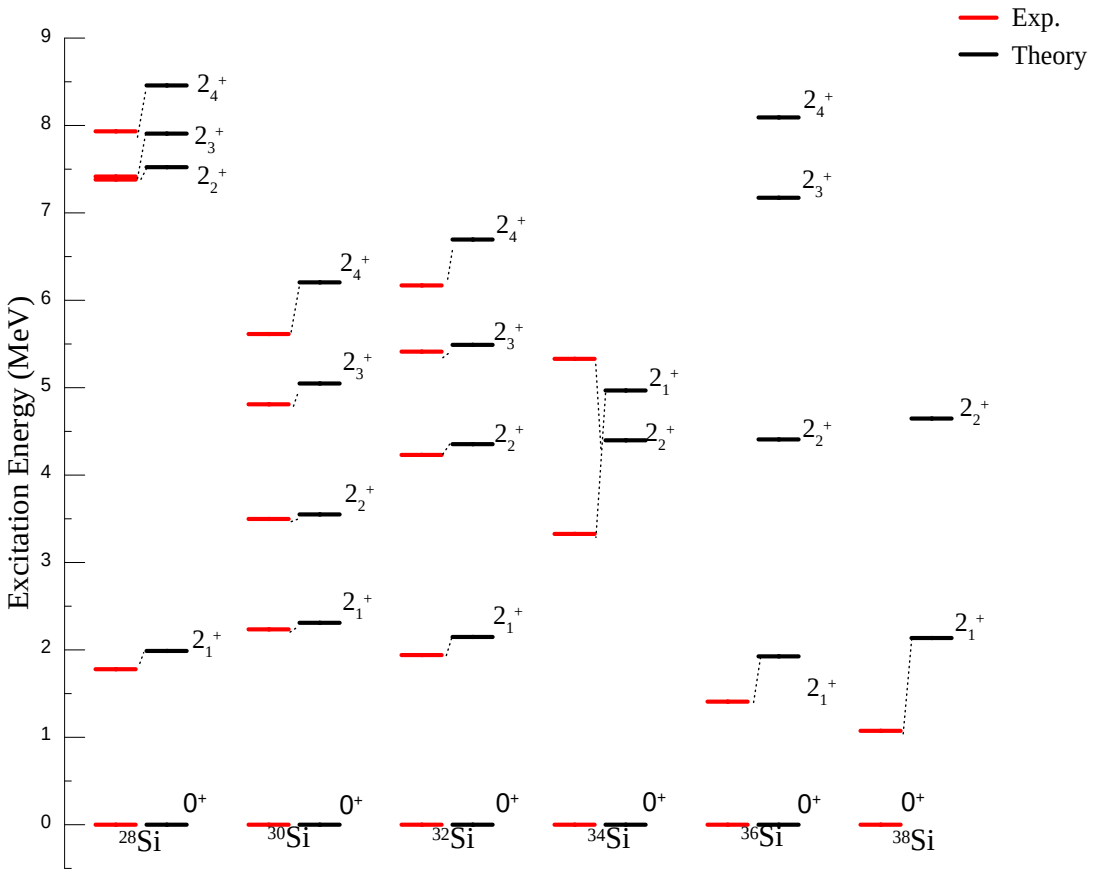

Fig.13: Experimental and theoretical energy levels for for low and higher-lying 2^+ states in even-even Si-isotopes.

Fig.14 (a) illustrates the systematic behavior of the electromagnetic transition probabilities $B(E2)$ in the Si isotopes chain which is drawn in comparison with the excitation energies (Fig.14(b)). It is obvious that the experimental data are in fairly good agreement with the calculated data from ^{28}Si to ^{34}Si but rapid deviation starts to occur with the experimental data, taken from Ref [35]. As the neutron number increases from N =12 (^{28}Si), the degree of collectivity smoothly and monotonically decreases until the closed shell is reached at N = 20 (^{34}Si). There is large discrepancy between the experimental $B(E2)$ and calculated values in the Si isotopes beyond N= 20 due to model space restriction which directly effects the excitation energy value as obvious in Fig.14.

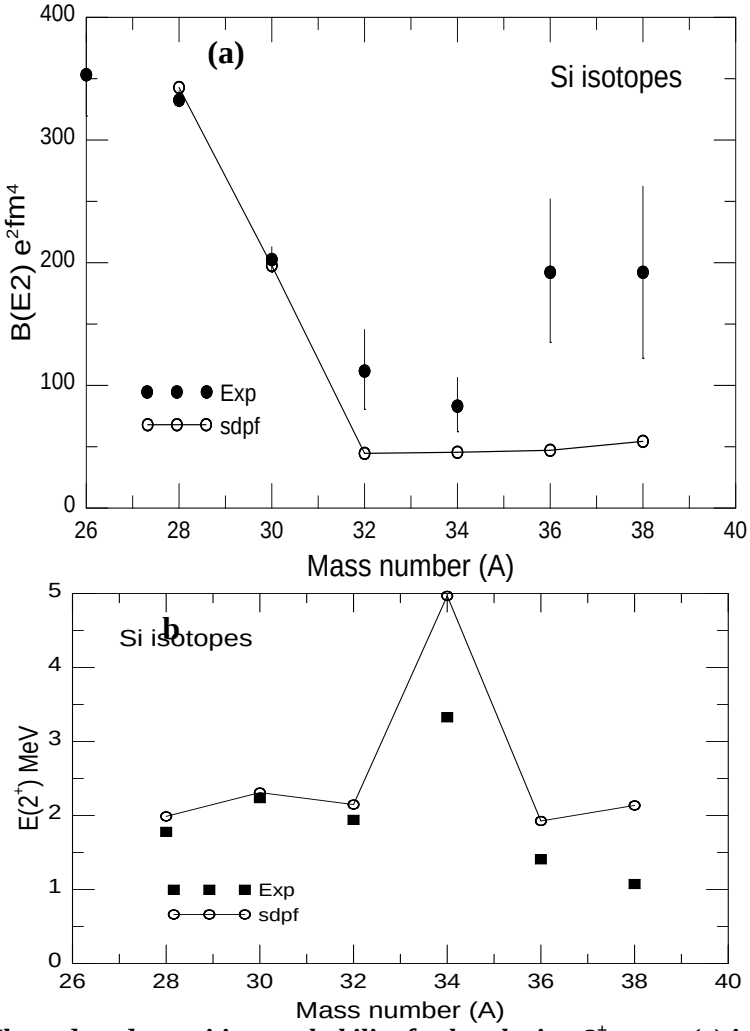

Fig.14: The reduced transition probability for low-laying 2^+ states (a) in comparison with excitation energy (b).

Conclusions

We have investigated the microscopic structures of $^{28\text{-}40}$Si-isotopes toward neutron dripline in the framework of the Skyrme-Hrtree-Fock method in the *sdpf* valence space using Skx25 and SLy4 Skyrme parameterizations. The calculations have introduced a reasonable agreement between measured and calculated binding energy, charge radii as well as charge densities .This proves that our method is accurate and sophisticated. This agreement is a key point for extrapolating of other quantities such as neutron and proton radii, skin thickness and pairing energies. The level scheme, S_{2n}, δ_{2n} of Si isotopes exhibit good agreement with all known experimental data. We were able to reproduce the main trends of the binding energies of Si isotopes from the stable to the neutron drip line isotopes. Another significant conclusion is that the two neutron shell gap δ_{2n}, and the pairing gap $\Delta 3n$ have the highest value in comparison with adjacent isotopes around N=16, 22 (^{30} Si, ^{36}Si) which indicates a new magic number and shell closure. Consequently, this quantity measure the size of the step found in the two-nucleon separation energy and, therefore, it is strongly peaked at magic shell closures. Moreover, the highest value of the pairing gap is occurred in N=20 (^{34}Si). Our results revealed that the two-neutron separation energy for ^{30}Si(N=16) and ^{36}Si (N=22) have relatively higher values than adjacent isotopes which indicates magicity and shell closure. The higher values of two neutron shell gap

δ_{2n} and pairing gap $\Delta 3n$ occurred for N=16, N=20, and N=22 which led us to conclude that N=16 and N=22 are a new magic numbers and shell closure.

Acknowledgments

The authors would like to express their thanks to the nuclear physics group in the department of physics, college of science, and university of Baghdad for their cooperation.

References

[1] S.Stoica, L.Trache, R.Tribble, Exotic Nuclei and Nuclear Particle Astrophysics (World Scientific Publishing, 2006).
[2] Kris L. G. Heyde, The Nuclear Shell Model, 2nd edn. (Springer, NY, 1994).
[3] T. H. R. Skyrme, Nucl. Phys., 9, 4 (1959) 615-634.
[4] E. Caurier, G. Martínez-Pinedo, F. Nowacki, A. Poves, A. P. Zuker, Rev. Mod. Phys., 77 (2005) 427-488.
[5] Yutaka Utsuno, Takaharu Otsuka, B. Alex Brown, Michio Honma, Takahiro Mizusaki, Noritaka Shimizu, Phy. Rev. C, 86 (2012) 05130-051301-5.
[6] X. Liang et al., Phy Rev. C 74, (2006) 014311-014311-6.
[7] R. W. Ibbotson, T. Glasmacher, B. A. Brown, L. Chen, M. J. Chromik, P.D. Cottle, M. Fauerbach, K. W. Kemper, D. J. Morrissey, H. Scheit, M. Thoennessen, Phy.Rev.Lett., 80, 10 (1998) 2081-2084.
[8] P. D. Cottle and K. W. Kemper, Phy. Rev. C, 66, (2002) 061301-061301-3.
[9] B J Cole, A. Watt, R. R Whitehead, J. Phys. A: Math., Nucl. Gen 7 (1974) 1399-1409.
[10] E. Caurier, F. Nowacki, A. Poves, Phy. Rev. C, 90 (2014) 014302-014302-9.
[11] P. Ring and P. Schuck, The Nuclear Many-Body Problem, 3rd edn. (Springer, NY, 2004).
[12] Vautherin and D. M. Brink, Phys. Rev. C, 5 (1972) 626-647.
[13] E. Suckling, MSc. Thesis,"Study of Magic Number Evoluation in exotic Nuclei", University of Surrey (2006).
[14] H. Sagawa, B. A. Brown, O. Scholten, Phys. Lett. B 159 (1985) 228-232.
[15] T. De Forest and J. D. Walecka, Adv. Phys. 15 (1966) 1-109.
[16] B. A. Brown, Lecture Notes in Nuclear Structure Physics, National Superconducting Cyclotron Laboratory and Department of Physics and Astronomy, Michigan State University, E.Lansing, MI 48824, 2005 (unpublished).
[17] B.A.Brown, Massent SE, J.Phys.G, 5 (1979) 1655-1698.
[18] Tapas Sil, S. K. Patra, B. K. Sharma, M. Centelles, X. Vinas, Phys.Rev.C, 69 (2004) 044315-044315-11.
[19] Bohr and B.R.Mottelson, Nuclear Structure, Vol.I (World Scientific, Singapore, 1988).
[20] W. D. M. Rae, NuShellX, http://www.garsington.eclipse.co.uk.
[21] B.A.Brown, Prog. Part. Nucl. Phys., 47 (2001) 517-599.
[22] J.wesseling B. A. Brown, W. A. Richter, R. Lindsay, Phys. Lett. B, 49 (2000) 483-489.
[23] I. Angeli, At. Data Nucl. Data Tab., 78 (2004) 69-95.
[24] National Nuclear Data Center (NNDC), https://www.nndc.bnl.gov/.
[25] A.E. Chabanat, P. Bonche, P. Haensel, J. Meyer, R. Schaeffer, Nucl. Phys. A 635 (1998) 231-242.
[26] P. G. Reinhard, D. J. Dean, W. Nazarewicz, J. Dobaczewski, J. A. Maruhn, M. R. Strayer, Phys. Rev. C, 60 (1999) 014316-014316-20.

[27] K. Langanke, J.A. Maruhn, S. E. Koonin, Computational Nuclear Physics 1 (Springer-Verlag 1991).
[28] M. Brack, C. Guet, H. B. Hakansson, Phys. Lett., 5 (1985) 277-292.
[29] H. Krivinea, J. Treinera, O. Bohigasa, Nucl. Phys. A, 336 (1980) 155-184.
[30] E.Caurier, F.Nowacki, A.Povas, Eur.Phys J.A, 15 (2002) 157-160.
[31] O.V. Bespalova, N.A. Fedorov, A.A. Klimochkina, M.L. Markova, T.I. Spasskaya, T.Yu. Tretyakova, Eur.Phys J.A, 54 (2018) 2-14.
[32] K.Kaneko, Y.Sun, T.Mizusaki, M.Hasegawa, Phys. Rev. C, 83 (2011) 014321-014321-10.
[33] O.Sorlin, "Shell Evolution and Nuclear Forces", (EDP science, 2014).
[34] P. Sarriguren, M. K. Gaidarov, E. Moya de Guerra, A. N. Antonov, Phys. Rev. C, 76 (2007) 044322-044322-13.